JOURNAL OF Materials CHEMISTRY

Unexpected substitution in the $Li_{1-3x}Fe_xNiPO_4$ ($0<x<0.15$) solid solution. Weak ferromagnetic behaviour

Aintzane Goñi,[a] Luis Lezama,[a] María Isabel Arriortua,[b] Gaston E. Barberis[a,c] and Teófilo Rojo*[a]

[a]*Dpto. Química Inorgánica,*
[b]*Dpto. Mineralogía-Petrología, F. Ciencias, UPV/EHU, Apdo. 644, Bilbao, Spain 48080. E-mail: qiproapt@lg.ehu.es*
[c]*Instituto de Física Gleb Wataghin, UNICAMP, Campinas (SP), Brazil 13087-970*

Received 30th September 1999, Accepted 22nd November 1999

$Li_{1-3x}Fe_xNiPO_4$ ($0<x<0.15$) solid solution phases have been synthesized by solid state reaction. X-Ray studies on polycrystalline samples show that all phases are isostructural with the parent $LiNiPO_4$ compound, crystallizing in the orthorhombic system, space group *Pnma*. The evolution of the lattice parameters with the iron content follows Vegard's law. The IR spectra show split bands for the phosphate groups, in good agreement with the distortion observed in the crystal structure. The EPR spectra for all phases show a broad band centred at zero field. The absence of a signal corresponding to Fe^{3+} ions suggests the presence of Fe^{III}–Ni^{II} interactions strongly affected by the zero field splitting of the nickel(II) ions. The magnetic behaviour of the $Li_{1-3x}Fe_xNiPO_4$ ($0<x<0.15$) phases can be described as antiferromagnetic with the presence of weak ferromagnetism below the ordering temperature. The magnitude of the remanent ferromagnetic moment is indicative of the existence of iron clustering in the samples. The FeO_6 octahedra form finite chains in which the magnetic moments of the Fe^{3+} ions are antiferromagnetically aligned with a small canting angle.

Introduction

The potential of phosphate compounds for optical, catalytic, magnetic or ionic conductivity applications is a driving force in the emergence of materials science.[1] In this realm, the search for solid electrolytes for the design of new lithium batteries is of substantial interest.[2] Lithium phosphates are good candidates in this area since they present the required chemical and thermal stability for technological applications,[3] and in many cases, excellent ionic conductivity.[4–8] Moreover, the phosphate compounds show an enormous variety of structural types[9,10] which favours the study of new families. The presence of magnetic transition metal ions in lithium phosphate materials allows the study of magnetic behaviour in these phases.

$LiNiPO_4$ crystallizes in a three-dimensional structure built by the stacking, along the [100] direction, of nickel phosphate layers.[11] Neutron diffraction studies have shown that the spin system associated with the Ni^{2+} ions in this compound undergoes a collinear antiferromagnetic ordering at $T_N = 19$ K, with the characteristics of coupled two-dimensional square planes.[12,13] However, the crystal structure of $LiNiPO_4$ can be considered as tubular with channels along the [010] and [001] directions, which are occupied by the Li^+ ions.

The characteristics of this crystal lattice suggest that the creation of vacancies in the Li positions will generate potential sites for ionic jumping, with expected enhancement of lithium mobility. One method to create such vacancies may be *via* substitution of Ni(II) ions [ionic radius (i.r.) = 83.0 pm] by a non-magnetic ion, with higher ionic charge and similar or smaller ionic radius, such as Al^{III} (i.r. = 67.5 pm) or Ga^{III} (i.r. = 76.0 pm). However, attemps to carry out substitution with these ions have been unsuccessful.

An attempt was thus made here to substitute Ni^{2+} for a 3d metal ion with chemical and geometrical similarities. A natural candidate was Fe^{3+}, and a strategy of synthesis was designed to obtain phases of the general formula $Li_{1-x}Ni_{1-x}Fe_xPO_4$. As high spin Fe^{III} has $S = 5/2$, its magnetic contribution to the lattice might be of interest. As observed with other ions, a mixture of phases was systematically obtained, with the presence of $Li_3Fe_2(PO_4)_3$ compound[14,15] in the final product. An increasing proportion of this phase was observed with the amount of iron added. Modification of the stoichiometry, in an attempt to eliminate this impurity in the reaction, led to $Li_{1-3x}Fe_xNiPO_4$ phases ($x = 0.033$, 0.067, 0.100, 0.133), in which each inserted Fe^{3+} ion unexpectedly displaces three lithium cations as result was confirmed by neutron diffraction studies (see ref. 13).

This article reports on the synthesis, structural study and spectroscopic and magnetic properties of the $Li_{1-3x}Fe_xNiPO_4$ ($0<x<0.15$) solid solution, showing the presence of iron clustering in these phases and the existence of an interesting magnetic phenomenon of weak ferromagnetism.

Experimental

Synthesis

The preparation of the $Li_{1-3x}Fe_xNiPO_4$ ($0<x<0.15$) phases was carried out by solid state synthesis. Stoichiometric amounts of the starting materials $Ni(NO_3)_2{\cdot}6H_2O$, $Fe(NO_3)_3{\cdot}9H_2O$, $(NH_4)H_2PO_4$ and $LiOH{\cdot}H_2O$ were mixed and homogenized in an agate mortar. The resultant mixtures were heated to 300 °C for 1 h, in order to decompose the nitrates. After a second homogenization in the mortar, the samples were calcined at 800 °C for 20 h, in air atmosphere.

The Li, Ni, Fe and P contents in the obtained products were analyzed by ICP (inductively coupled plasma) analytical emission spectroscopy. The experimental results for each sample and the theoretical values corresponding to the proposed formulae are given in Table 1.

Physical measurements

Analytical measurements were carried out by ICP-AES analysis, with an ARL 3410+ICP instrument with Minitorch equipment. IR spectra were measured with a Nicolet FT-

Table 1 Experimental (theoretical) analytical data (%) obtained for the $Li_{1-3x}Fe_xNiPO_4$ ($0<x<0.15$) compounds

Compound	Li	Fe	Ni	P
$Li_{0.9}Fe_{0.033}NiPO_4$	3.8 (3.86)	1.1 (1.15)	36.3 (36.29)	18.9 (19.14)
$Li_{0.8}Fe_{0.067}NiPO_4$	3.4 (3.41)	2.2 (2.30)	35.9 (36.02)	18.9 (19.01)
$Li_{0.7}Fe_{0.100}NiPO_4$	3.0 (2.96)	3.4 (3.40)	35.6 (35.77)	18.8 (18.87)
$Li_{0.6}Fe_{0.133}NiPO_4$	2.5 (2.52)	4.5 (4.50)	35.4 (35.52)	18.6 (18.74)

IR 740 spectrometer using the KBr disk technique. EPR spectra were recorded on powdered samples at X-band frequency with a Bruker ESP300 spectrometer equipped with standard Oxford low-temperature device and calibrated by an NMR probe for the magnetic field. The frequency was measured with a HP 5352B microwave frequency counter. Magnetic measurements in the temperature range 1.8–300 K were obtained at a variety of magnetic fields using a Quantum Design MPMS-7 SQUID magnetometer.

Structure refinement of $Li_{1-3x}Fe_xNiPO_4$ ($0<x<0.15$)

The X-ray powder diffraction patterns of the $Li_{1-3x}Fe_xNiPO_4$ ($0<x<0.15$) phases were measured at room temperature on a Stoe diffractometer using Ge-monochromated Cu-Kα_1 radiation. The data were collected in the 2θ range 5–70°, in steps of 0.02°. A small impurity peak was detected at 2θ *ca.* 16.5° in the spectra of some phases. Rietveld refinement of the crystal structures was undertaken by starting from the structural model of $LiNiPO_4$.[11] The structures were refined using the FULLPROF program[16] with a pseudo-Voigt function used to model the peak shape. An asymmetry correction was applied to the low-angle reflections. Scale and background variables were refined initially, followed in subsequent iterations, by the zero point of 2θ, the cell constants, the peak shape parameters, the atomic parameters, the overall isotropic temperature factors and the occupation factors of the Li and Fe atoms. During the process, a restriction in which each Fe^{3+} ion removes three Li^+ cations from their sites was employed.

The reliability factors in each case dropped, by successive refinement cycles, to the values shown in Table 2. Fig. 1 shows the observed, calculated and difference powder X-ray diffraction (XRD) patterns of the four studied $Li_{1-3x}Fe_xNiPO_4$ phases. The final fractional atomic coordinates, temperature and occupation factors and selected interatomic distances and angles are given in Tables 3 and 4.

Results and discussion

Crystal structures of the $Li_{1-3x}Fe_xNiPO_4$ ($0<x<0.15$) phases

The $Li_{1-3x}Fe_xNiPO_4$ phases are isostructural with the parent $LiNiPO_4$ compound. The nickel(II) ions are distributed in approximately square-planar layers, and linked together by oxygen atoms from the phosphate groups. The three-dimensional structure is built by the packing of the nickel phosphate sheets parallel to the (100) plane, connected through the PO_4 groups along the perpendicular [100] direction. The resulting crystal net shows the presence of longitudinal channels along the [010] direction, in which the Li^+ and Fe^{3+} ions, together with the vacancies, are located (Fig. 2).

The cell parameters of the $Li_{1-3x}Fe_xNiPO_4$ compounds show variation with the degree of iron substitution, x (Fig. 3). Evolution of the cell parameters is linear in all cases following Vegard's law; the b parameter diminishes with iron insertion, whereas the a and c parameters increase and the cell volume increases with Fe^{3+} insertion. Considering that the effective ionic radius of the high spin Fe^{3+} cation in octahedral coordination is 78.5 pm, and that corresponding to the hexacoordinated Li^+ ion is 90.0 pm, a reduction of the cell volume might have been expected with the substitution of Li^+ by Fe^{3+}. However, it must be considered that vacancies are also introduced in Li^+ sites causing repulsion between negatively charged ions and consequently, an expansion of the crystal net.

The NiO_6 octahedra are highly distorted in all the compounds showing large ranges of both Ni–O bond distances and O–Ni–O angles. The Ni(II) ion and the axial O(1) and O(2) atoms are located at special positions in the (010) mirror plane (Fig. 2) with the O atoms being responsible for interlayer connection through the PO_4 groups. The equatorial atoms of the NiO_6 groups are four symmetry-related O(3) atoms, O(3), $O(3)^i$, $O(3)^{ii}$ and $O(3)^{iii}$ (i = $1/2-x$, $-y$, $1/2+z$; ii = x, $1/2-y$, z; iii = $1/2-x$, $1/2+y$, $1/2+z$) which, owing to their position out of the (010) mirror plane, define a plane perpendicular to *ac*. In each octahedron, two O(3) atoms belong to the same phosphate group while the remaining pair of O(3) atoms are from the other two adjacent phosphate groups. There are two sets of two identical Ni–O(3) equatorial bonds (Table 4) while the O(3)–Ni–O(3) angles are significantly different from 90°. However, the sum of the four O(3)–Ni–O(3) equatorial angles is 360° indicative of the planarity of the oxygen atoms and the Ni(II) ion. The apical oxygens, O(1) and O(2), deviate from the 'vertical', with O(1)–Ni–O(2) angles of *ca.* 177.5°.

The LiO_6 (or FeO_6) octahedra exhibit C_i symmetry leading to three independent Li–O distances, ranging from 2.079(2) to 2.158(3) Å, and three O–Li–O angles of 180°. The remainder of the O–Li–O substantially deviate from 90° (Table 4). The adjacent LiO_6 octahedra are connected by the O(1) and O(2) vertexes in edge-sharing chains along the [010] direction.

Finally, PO_4 groups are formed by distorted tetrahedra with P–O distances (1.517–1.565 Å) and O–P–O angles (101.6–114.9°) showing significant ranges in all phases. The phosphorus, O(1) and O(2) atoms lie in the *ac* mirror plane, whereas the other two O(3) atoms are symmetry-related by reflection in this plane. The P–O(2) and P–O(3) distances are similar but longer than the P–O(1) bond. The O(3)–P–O(3) angle (*ca.* 102°), formed by the O(3) atoms of the same NiO_6 polyhedron, is smaller than the other O–P–O angles (112.1–114.9°).

Table 2 Crystal parameters and details of the refinement of the structure of $Li_{1-3x}Fe_xNiPO_4$ ($x=0.033$, 0.067, 0.100, 0.133)[a]

	$Li_{0.9}Fe_{0.033}NiPO_4$	$Li_{0.8}Fe_{0.067}NiPO_4$	$Li_{0.7}Fe_{0.1}NiPO_4$	$Li_{0.6}Fe_{0.133}NiPO_4$
a/Å	10.030(1)	10.033(1)	10.038(1)	10.040(1)
b/Å	5.853(1)	5.846(1)	5.840(1)	5.835(1)
c/Å	4.681(1)	4.687(1)	4.691(1)	4.695(1)
R_F (%)	4.30	5.59	3.61	5.55
R_B (%)	3.99	4.54	3.56	4.68
R_p (%)	7.73	7.32	5.91	5.72
R_{wp} (%)	10.5	10.1	7.66	7.44
χ^2	1.75	2.07	1.41	1.50

[a]Details in common: orthorhombic crystal system, space group *Pnma* (no. 62), $Z=4$.

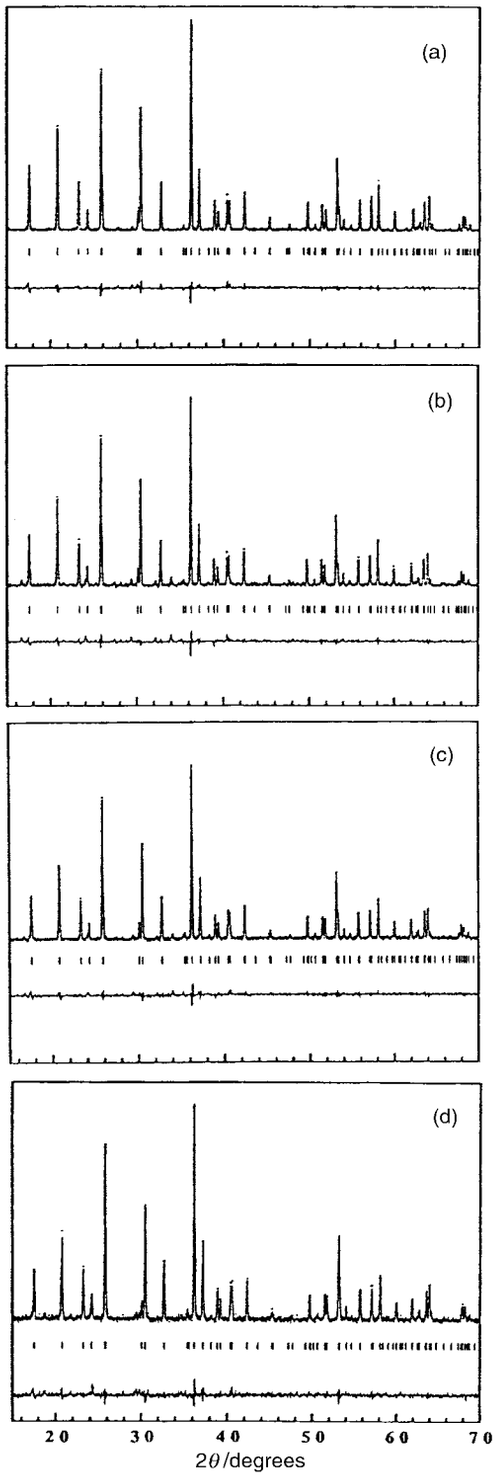

Fig. 1 Observed, calculated and difference powder XRD patterns of (a) $Li_{0.9}Fe_{0.033}NiPO_4$, (b) $Li_{0.8}Fe_{0.067}NiPO_4$, (c) $Li_{0.7}Fe_{0.100}NiPO_4$ and (d) $Li_{0.6}Fe_{0.133}NiPO_4$.

IR spectroscopy

IR spectra of the $Li_{1-3x}Fe_xNiPO_4$ ($0<x<0.15$) phases together with that of $LiNiPO_4$ for comparison are shown in Fig. 4. All the compounds exhibit similar spectra in good agreement with the structural results.

The strong and split band appearing at *ca.* 1060 cm^{-1} for all compounds is attributed to the stretching vibration mode of the PO_4 groups.[17] The splitting of this band is caused by the distortion of the phosphate tetrahedra as observed from the structural results. The $\nu(PO_4)$ band exhibits a progressive broadening with increased amount of Fe^{3+} in the compounds

Table 3 Fractional atomic coordinates, occupancies and temperature factors ($Å^2$) for $Li_{1-3x}Fe_xNiPO_4$ ($x=0.033$, 0.067, 0.100, 0.133)

	x	y	z	Occ.	B_{eq}
$Li_{0.9}Fe_{0.033}NiPO_4$					
Li	0.0	0.0	0.0	0.930(1)	1.5(6)
Fe	0.0	0.0	0.0	0.024(1)	0.3
Ni	0.276(1)	0.25	0.981(1)	1.0	0.3
P	0.095(1)	0.25	0.418(1)	1.0	0.5
O(1)	0.102(1)	0.25	0.742(1)	1.0	0.7
O(2)	0.451(1)	0.25	0.202(1)	1.0	0.7
O(3)	0.165(1)	0.042(1)	0.277(1)	1.0	0.7
$Li_{0.8}Fe_{0.067}NiPO_4$					
Li	0.0	0.0	0.0	0.822(1)	1.8(9)
Fe	0.0	0.0	0.0	0.060(1)	0.3
Ni	0.276(1)	0.25	0.981(1)	1.0	0.3
P	0.095(1)	0.25	0.418(1)	1.0	0.5
O(1)	0.099(1)	0.25	0.742(2)	1.0	0.7
O(2)	0.450(1)	0.25	0.198(2)	1.0	0.7
O(3)	0.165(1)	0.044(1)	0.275(1)	1.0	0.7
$Li_{0.7}Fe_{0.100}NiPO_4$					
Li	0.0	0.0	0.0	0.678(1)	2.6(9)
Fe	0.0	0.0	0.0	0.108(1)	0.3
Ni	0.275(1)	0.25	0.981(1)	1.0	0.3
P	0.094(1)	0.25	0.418(1)	1.0	0.5
O(1)	0.100(1)	0.25	0.741(2)	1.0	0.7
O(2)	0.459(1)	0.25	0.193(2)	1.0	0.7
O(3)	0.166(1)	0.044(1)	0.277(1)	1.0	0.7
$Li_{0.6}Fe_{0.133}NiPO_4$					
Li	0.0	0.0	0.0	0.574(2)	2.8(9)
Fe	0.0	0.0	0.0	0.142(2)	0.3
Ni	0.276(1)	0.25	0.983(1)	1.0	0.3
P	0.095(1)	0.25	0.417(1)	1.0	0.5
O(1)	0.101(1)	0.25	0.742(2)	1.0	0.7
O(2)	0.449(1)	0.25	0.199(2)	1.0	0.7
O(3)	0.165(1)	0.046(1)	0.276(1)	1.0	0.7

possibly indicative of an increase of disorder in the structures, as a consequence of the substitution of a part of the Li^+ ions by Fe^{3+} cations and vacancies. The bending mode of the PO_4 group appears as a split signal at *ca.* 600 cm^{-1}. While the position of this band is not modified with the amount of iron in the compounds it does undergo gradual broadening.

EPR and magnetic properties

X-Band EPR spectra of the four $Li_{1-3x}Fe_xNiPO_4$ ($x=0.033$, 0.067, 0.100, 0.133) polycrystalline samples were measured in the temperature range 4.2–300 K and similar spectra were obtained for all the compounds. A very broad band is observed approximately at zero field, which is characteristic of Ni^{2+} compounds with the energy of zero field splitting values, D, greater than the microwave energy employed in the measure-

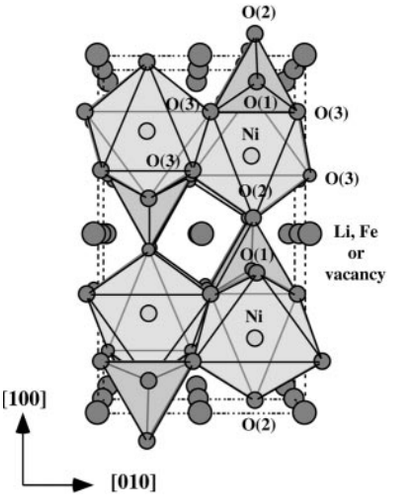

Fig. 2 Crystal structure of the $Li_{1-3x}Fe_xNiPO_4$ ($0<x<0.15$) phases.

Table 4 Selected distances (Å) and angles (°) for $Li_{1-3x}Fe_xNiPO_4$ ($x=0.033$, 0.067, 0.100, 0.133)[a]

	$Li_{0.9}Fe_{0.033}NiP$	$Li_{0.8}Fe_{0.067}NiP$	$Li_{0.7}Fe_{0.1}NiP$	$Li_{0.6}Fe_{0.133}NiP$
Li coordination octahedra				
Li–O(1) ×2	2.158(3)	2.142(2)	2.150(3)	2.148(3)
Li–O(2) ×2	2.079(2)	2.094(2)	2.112(2)	2.095(2)
Li–O(3) ×2	2.120(3)	2.116(3)	2.127(3)	2.122(3)
O(1)–Li–O(2)	89.4(1)	89.1(1)	88.4(1)	88.7(1)
O(1)–Li–O(3)	83.8(1)	84.1(1)	84.0(1)	83.6(1)
O(2)–Li–O(3)	72.1(1)	72.0(1)	71.9(1)	72.1(1)
Ni coordination octahedra				
Ni–O(1)	2.070(4)	2.095(4)	2.085(4)	2.088(4)
Ni–O(2)	2.042(4)	2.026(4)	2.011(4)	2.011(4)
Ni–O(3) ×2	2.152(3)	2.140(3)	2.142(3)	2.131(3)
Ni–$O(3)^{i}$ ×2	2.044(3)	2.058(3)	2.051(3)	2.069(3)
O(1)–Ni–O(2)	177.8(1)	177.9(2)	177.0(2)	177.7(2)
O(3)–Ni–$O(3)^{i}$	88.6(1)	88.9(1)	88.8(1)	89.2(1)
O(3)–Ni–$O(3)^{ii}$	69.0(1)	68.5(1)	68.4(1)	67.8(1)
Phosphate tetrahedra				
P–O(1)	1.520(4)	1.517(4)	1.518(4)	1.528(4)
P–O(2)	1.544(4)	1.553(4)	1.544(4)	1.565(4)
P–O(3) ×2	1.557(3)	1.549(3)	1.551(3)	1.534(3)
O(1)–P–O(2)	114.2(2)	112.2(2)	112.1(2)	112.7(2)
O(1)–P–O(3)	113.6(1)	114.9(1)	114.0(1)	114.5(1)
O(3)–P–$O(3)^{ii}$	103.0(2)	102.1(2)	101.9(2)	101.6(2)

[a]Symmetry translations: i = 1/2−x, −y, 1/2+z; ii = x, 1/2−y, z.

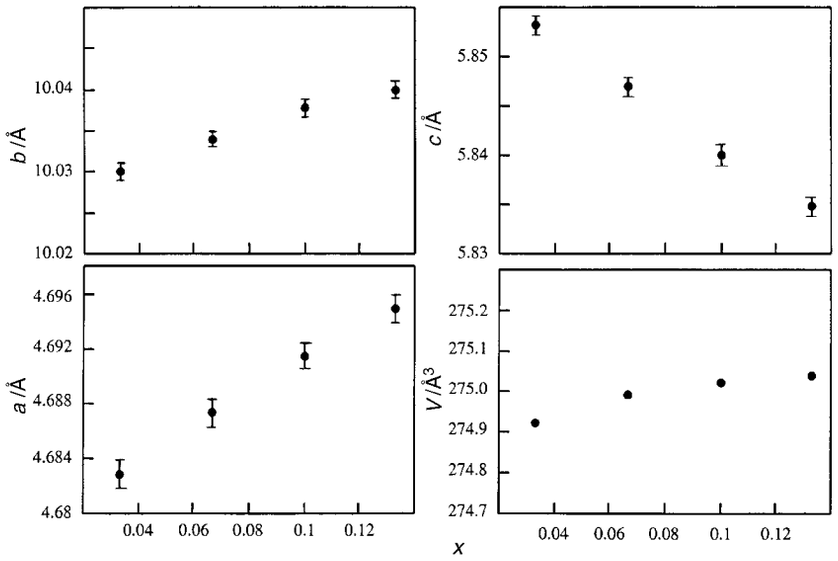

Fig. 3 Evolution of the cell parameters with the iron content, x, for the $Li_{1-3x}Fe_xNiPO_4$ ($0<x<0.15$) phases.

ments.[18] The absence of bands corresponding to the Fe^{3+} ions allows us to deduce that the Fe^{3+} and Ni^{2+} ions are coupled in the measured temperature range, with the characteristics of the Ni^{2+} ions being predominant. The Fe–Ni magnetic interactions must be strong and long range since the coupling is also observed at room temperature.

The study of the thermal evolution of the molar magnetic susceptibility in the $Li_{1-3x}Fe_xNiPO_4$ ($x=0.033$, 0.067, 0.100, 0.133) phases was carried out in the temperature range 5–300 K with a magnetic field of 0.1 T. The χ_m and $\chi_m T$ *vs.* T curves of all the compounds are shown in Fig. 5. A maximum centred at 25 K is observed for χ_m for all phases, which is similar to that observed for $LiNiPO_4$.[19] However, in the solid solution, unlike in the $LiNiPO_4$ phase, an abrupt increase of the χ_m values is observed at temperatures lower than that of the maximum. This result can be attributed to the appearance of a ferromagnetic component below the ordering temperature. The experimental data do not obey the Curie–Weiss law over the studied temperature range. The thermal evolution of the product $\chi_m T$ shows a continuous reduction in values from

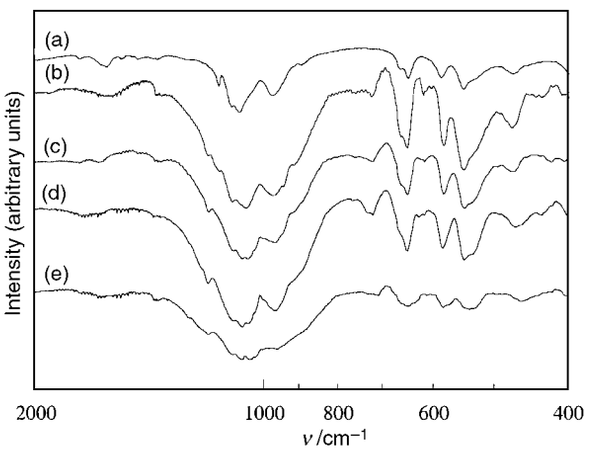

Fig. 4 IR spectra of (a) $LiNiPO_4$, (b) $Li_{0.9}Fe_{0.033}NiPO_4$, (c) $Li_{0.8}Fe_{0.067}NiPO_4$, (d) $Li_{0.7}Fe_{0.100}NiPO_4$ and (e) $Li_{0.6}Fe_{0.133}NiPO_4$.

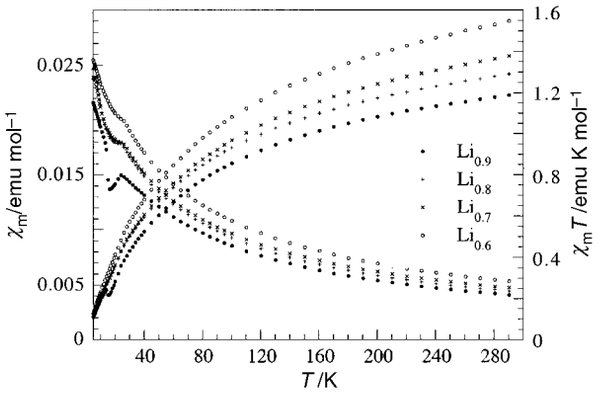

Fig. 5 Thermal evolution of χ_m and $\chi_m T$ for the $Li_{1-3x}Fe_xNiPO_4$ ($x=0.033$, 0.067, 0.100, 0.133) phases, in the temperature range 5–300 K, at a magnetic field of 0.1 T.

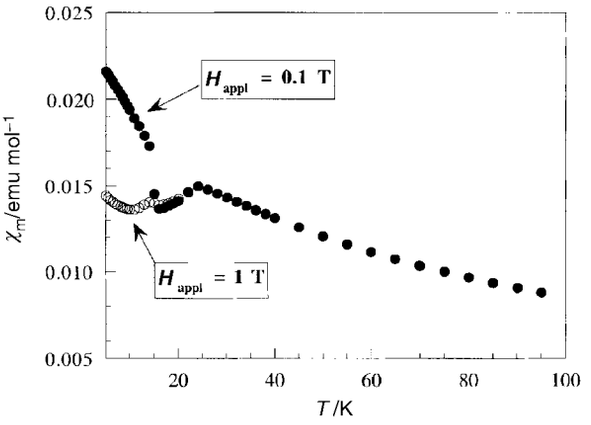

Fig. 7 Thermal evolution of χ_m for the $Li_{0.9}Fe_{0.033}NiPO_4$ phase at magnetic fields of 0.1 and 1 T.

room temperature (Fig. 5), indicating the existence of predominant antiferromagnetic interactions. The $\chi_m T$ value at 300 K is proportional to the amount of Fe(III) in the phase.

The magnetization *vs.* field curve measured at 5 K for $Li_{0.9}Fe_{0.033}NiPO_4$ exhibits a hysteresis loop, becoming nearly linear up to 0.2 T (Fig. 6). A weak magnetization of *ca.* 4.9 emu mol^{-1} is maintained at zero field. The observed value for the coercitive field is *ca.* -100×10^{-4} T. These results indicate the presence of weak ferromagnetism below T_N, this being similar in all substituted phases.

In order to carry out a deeper study of the magnetic behaviour in this solid solution, the thermal evolution of χ_m in the $Li_{0.9}Fe_{0.033}NiPO_4$ phase was measured at low temperatures and at different magnetic fields, from 0.1 to 1 T (Fig. 7). The χ_m values are similar above 25 K for all magnetic fields. However, at around and below 15 K the results obtained are very different. The stronger magnetic fields smooth the rise of χ_m when T is decreased, removing the extra peak. This effect is characteristic of a canting phenomenon, in which the weak remanent magnetization is provided by a not exactly collinear antiferromagnetic arrangement of the magnetic moments.

Discussion and conclusions

The magnetic structure of $LiNiPO_4$ indicates four different nickel positions in the unit cell, with all the magnetic moments antiferromagnetically coupled along the *c* direction (see refs. 12 and 13). Considering the similarity between the crystal structures of the $Li_{1-3x}Fe_xNiPO_4$ phases and that corresponding to $LiNiPO_4$, together with the maximum value observed in χ_m (which corresponds to the antiferromagnetic arrangement of the nickel ions, remaining unchanged for the solid-solution

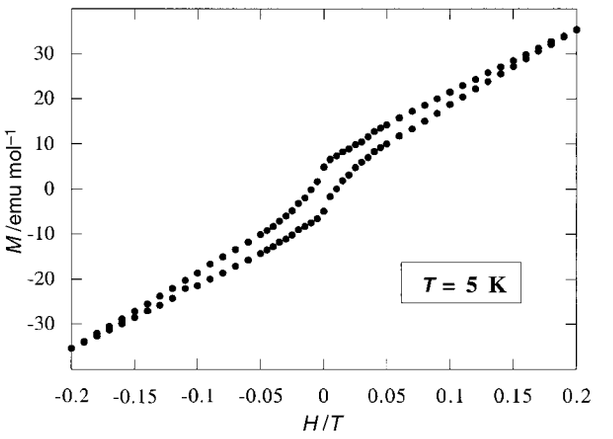

Fig. 6 Magnetization *vs.* field hyteresis loop at $T=5$ K for $Li_{0.9}Fe_{0.033}NiPO_4$.

compounds), one can conclude that the Ni(II)–Ni(II) interactions do not undergo any significant change with iron substitution. The NiO_6 octahedra, vertex-sharing on the *bc* crystallographic plane, establish an antiferromagnetic exchange pathway Ni–O–Ni *via* $d_{x^2-y^2}$ orbitals. An exchange pathway along the [100] direction can also be considered through the PO_4 groups, involving the d_{z^2} orbitals of the Ni(II) ions and leading also to antiferromagnetic interactions.

The insertion of a percentage of Fe^{3+} ions in Li^+ ion positions affords a new magnetic exchange pathway Ni–O–Fe–O–Ni along the [100] direction, with heterometallic character. The EPR measurements showed the existence of long range Fe^{3+}–Ni^{2+} interactions. These interactions should occur *via* the Ni^{2+} ions of two adjacent (011) layers through the Fe^{3+} ions, increasing the three-dimensional character of the magnetic behaviour. However, this apparently does not affect the final distribution of the nickel moments in the magnetic ordered state.

The weak ferromagnetic moment present in theses systems could be attributed to the non-cancellation of the iron moments homogeneously distributed in the crystal lattice. However, this hypothesis is not consistent with the experimental data. First, the magnitude of the observed remanent magnetization (*ca.* 0.001 μ_B for $Li_{0.9}Fe_{0.033}NiPO_4$) is much smaller than the corresponding value expected for the iron concentration in the sample (0.033 Fe^{3+} mol $\times$ 5.92 μ_B mol^{-1} (high spin Fe^{3+}) = 0.20 μ_B); and second, the remanent magnetization disappears at high magnetic fields. Thus, the observed weak ferromagnetism appears to correspond to canting phenomena between antiferromagnetically coupled Fe^{3+} moments. This fact can be explained either as due to the presence of iron clustering in the crystal lattice, despite an expected random distribution of Fe^{3+} ions in the samples, or a slight misalignment of the Ni magnetic moments owing to the presence of the Fe ions. However, preliminary results concerning the magnetic study on the related $Li_{1-3x}Fe_xMgPO_4$ phase indicate the existence of Fe–Fe antiferromagnetic couplings. Consequently, we can deduce that the effects observed in the present phases can be attributed to the presence of iron clustering.

The Fe^{3+} clusters can be considered as finite chains of FeO_6 octahedra, edge-shared along the [010] direction. As was observed in the structural study, the octahedra along the chains are successively tilted with respect to each other, because they are symmetry related by the (010) mirror plane. This fact is characteristic of the existence of canting (see ref. 18), fulfilling the required absence of a centre of symmetry between the magnetic ions. Iron clusters can be associated with the presence of holes in some regions of the lattice with charge balance maintained by the presence of Li^+ cations in other regions of the crystal. The ionic mobility of the Li^+ ions would be reduced

due to the presence of clustered Fe^{3+} ions which hamper the access of the Li^{+} ions to created vacancies.

Acknowledgements

This work has been carried out with the financial support of the Ministerio de Educación y Ciencia (PB97-0640) and the UPV/EHU (UPV 169.310-EB149/98) which we gratefully acknowledge.

References

1 A. K. Cheetam, *Science*, 1994, **264**, 794.
2 C. Julien and G. A. Nazri, *Solid State Batteries: Materials Design and Optimization*, Kluwer Academic Publishers, Boston, MA, 1994.
3 T. Kanazawa, *Inorganic Phosphate Materials*, Elsevier, Tokyo, 1989.
4 C. Masquelier, A. K. Padhi, K. S. Nanjundaswamy and J. B. Goodenough, *J. Solid State Chem.*, 1998, **135**, 228.
5 H. Aono, N. Imanaka and G. Y. Adachi, *Acc. Chem. Res.*, 1994, **27**, 265.
6 S. Ikeda, K. Nomura, K. Ito and H. Einaga, *Solid State Ionics*, 1994, **70**(71), 153.
7 J. Kuwano, N. Sato, M. Kato and K. Takano, *Solid State Ionics*, 1994, **70**(71), 332.
8 M. Casciola, in *Comprehensive Supramolecular Chemistry*, ed. G. Alberti and T. Bein, Elsevier, Oxford, 1996.
9 K. H. Lii, Y. F. Huang, V. Zima, C. Y. Huang, H. M. Lin, Y. C. Jiang, F. L. Liao and S. L. Wang, *Chem. Mater.*, 1998, **10**, 2599.
10 J. O. Nriagu and P. B. Moore, *Phosphate Minerals*, Springer-Verlag, Berlin, 1984.
11 I. Abrahams and K. S. Easson, *Acta Crystallogr., Sect. C*, 1993, **49**, 925.
12 R. P. Santoro, D. J. Segal and R. E. Newham, *J. Phys. Chem. Solids*, 1966, **22**, 1192.
13 D. Vaknin, J. L. Zarestky, J. E. Ostenson, B. C. Chakoumakos, A. Goñi, P. Pagliuso, T. Rojo and G. E. Barberis, *Phys. Rev. B: Condens. Matter*, 1999, **60**, 1100.
14 A. B. Bykov, A. P. Chirkin, L. N. Demyanets, S. N. Doronin, E. A. Genkina, A. K. Ivanov-Shits, I. P. Kondratyuk, B. A. Maksimov, O. K. Mel'nikov, L. N. Muradyan, V. I. Simonov and V. A. Timofeeva, *Solid State Ionics*, 1990, **38**, 31.
15 A. Goñi, L. Lezama, N. O. Moreno, L. Fournes, R. Olazcuaga, G. E. Barberis and T. Rojo, *Chem. Mater.*, 1999, in press.
16 J. Rodriguez Carvajal, FULLPROF Program. Rietveld Pattern Matching Analysis of Powder Patterns, 1994.
17 K. Nakamoto, *Infrared Spectra of Inorganic and Coordination Compounds*, John Wiley & Sons, New York, 1986.
18 R. L. Carlin, *Magnetochemistry*, Springer-Verlag, Berlin, 1986.
19 A. Goñi, L. Lezama, G. E. Barberis, J. L. Pizarro, M. I. Arriortua and T. Rojo, *J. Magn. Magn. Mater.*, 1996, **164**, 251.

Paper a907862b